

UCSF

UC San Francisco Previously Published Works

Title

Insertional Mutagenesis Identifies a STAT3/Arid1b/ β -catenin Pathway Driving Neurofibroma Initiation.

Permalink

<https://escholarship.org/uc/item/598976wb>

Journal

Cell Reports, 14(8)

Authors

Wu, Jianqiang
Keng, Vincent
Patmore, Deanna
et al.

Publication Date

2016-03-01

DOI

10.1016/j.celrep.2016.01.074

Peer reviewed



Published in final edited form as:

Cell Rep. 2016 March 1; 14(8): 1979–1990. doi:10.1016/j.celrep.2016.01.074.

Insertional mutagenesis identifies a STAT3/Arid1b/ β -catenin pathway driving neurofibroma initiation

Jianqiang Wu¹, Vincent Keng^{3,4,5,†}, Deanna M. Patmore¹, Jed K. Kendall¹, Ami V. Patel¹, Edwin Jousma¹, Walter J. Jessen¹, Kwangmin Choi¹, Barbara R. Tschida^{3,5}, Kevin A. T. Silverstein⁶, Danhua Fan⁶, Eric B. Schwartz⁷, James R. Fuchs⁷, Yuanshu Zou², Mi-Ok Kim², Eva Dombi⁸, David E. Levy⁹, Gang Huang¹, Jose A. Cancelas^{1,10}, Anat O. Stemmer-Rachamimov¹¹, Robert J. Spinner¹², David A. Largaespada^{3,4,5}, and Nancy Ratner^{1,*}

¹Division of Experimental Hematology and Cancer Biology, Cancer and Blood Diseases Institute, Cincinnati Children's Hospital Research Foundation, Cincinnati Children's Hospital, University of Cincinnati, Cincinnati, OH 45229, USA

²Division of Biostatistics and Epidemiology, Cincinnati Children's Hospital Research Foundation, Cincinnati Children's Hospital, University of Cincinnati, Cincinnati, OH 45229, USA

³Masonic Cancer Center, University of Minnesota, Minneapolis, MN 55455, USA

⁴Department of Genetics, Cell Biology and Development, University of Minnesota, Minneapolis, MN 55455, USA

⁵Center for Genome Engineering, University of Minnesota, Minneapolis, MN 55455, USA

⁶Biostatistics and Informatics, University of Minnesota, Minneapolis, MN 55455, USA

⁷Ohio State University, College of Pharmacy, Columbus, OH 43210, USA

⁸Pediatric Oncology Branch, National Cancer Institute, Bethesda, MD 20892, USA

⁹Department of Pathology and New York University Cancer Institute, New York, University School of Medicine, 550 First Avenue, New York, NY 10016, USA

¹⁰Hoxworth Blood Center, College of Medicine, University of Cincinnati, Cincinnati, OH 45229, USA

*Correspondence: nancy.ratner@cchmc.org, Phone: (513) 636-9469.

†Present address: Department of Applied Biology and Chemical Technology, the Hong Kong Polytechnic University, Hung Hom, Kowloon, Hong Kong.

Author Contributions

Conception and design: N.R. and D.A.L.

Acquisition of data: J.W., V.K., D.M.P., J.K.K., A.V.P., E.J., W.J.J., K.C., B.R.T., K.T.S., D.F., E.D., G.H., J.A.C., A.O.S.

Provided resources: E.B.S. and J.R.F. FLLL32; D.E.L., Stat3^{fl/fl} mouse, R.J.S., human samples.

Analysis and interpretation of data (including statistical analysis): J.W., V.K., Y.Z., M.K., N.R., D.A.L.

Writing and review the manuscript: J.W., V.K., N.R., D.A.L.

The authors declare no conflict of interest.

Publisher's Disclaimer: This is a PDF file of an unedited manuscript that has been accepted for publication. As a service to our customers we are providing this early version of the manuscript. The manuscript will undergo copyediting, typesetting, and review of the resulting proof before it is published in its final citable form. Please note that during the production process errors may be discovered which could affect the content, and all legal disclaimers that apply to the journal pertain.

¹¹Department of Pathology, Massachusetts General Hospital and Harvard Medical School, Boston, MA, 02114, USA

¹²Department of Neurologic Surgery, Mayo Clinic, Rochester, MN 55905, USA

Summary

To identify genes and signaling pathways that initiate Neurofibromatosis type 1 (*Nf1*) neurofibroma, we used unbiased insertional mutagenesis screening, mouse models, and molecular analyses. We mapped an *Nf1-Stat3-Arid1b/β-catenin* pathway which becomes active in the context of *Nf1* loss. Genetic deletion of *Stat3* in Schwann cells progenitors (SCPs) and Schwann cells (SCs) prevents neurofibroma formation, decreasing SCP self-renewal and β-catenin activity. β-catenin expression rescues effects of *Stat3* loss in SCs. Importantly, P-STAT3 and β-catenin expression correlate in human neurofibromas. Mechanistically, P-Stat3 represses *Gsk3β* and the SWI/SNF gene *Arid1b*, to increase β-catenin. Knock-down of *Arid1b* or *Gsk3β* in *Stat3^{fl/f};Nf1^{fl/fl};DhhCre* SCs rescues neurofibroma formation after in vivo transplantation. *Stat3* represses *Arid1b* through histone modification in a *Brg1* dependent manner, indicating that epigenetic modification plays a role in early tumorigenesis. Our data map a neural tumorigenesis pathway, and support testing JAK/STAT and Wnt/β-catenin pathway inhibitors in neurofibroma therapeutic trials.

eTOC Blurb

Wu et al map an *Nf1-Stat3-Arid1b/β-catenin* pathway that initiates Neurofibromatosis type 1 (*Nf1*) neurofibroma, using unbiased insertional mutagenesis screening. *Stat3* transcriptionally represses *Gsk3β* and *Arid1b*, thereby activating β-catenin in Schwann cell precursors - resulting in neurofibroma initiation and maintenance. *Stat3* mediated epigenetic modification plays a role in early tumorigenesis.

Introduction

Neurofibromas are benign peripheral nerve tumors that cause significant morbidity by disfigurement and tissue compression, and mortality if they compress vital organs (Boyd et al., 2009). Neurofibromas are a major feature of Neurofibromatosis type 1 (*NF1*), a common autosomal dominant disorder affecting about 1 in 3500 individuals. Surgery remains the mainstay of neurofibroma therapy but is rarely curative, so new treatments are urgently needed.

Peripheral nerve Schwann cells (SCs) are the primary pathogenic cell in neurofibromas, as biallelic mutation/loss of *NF1* occurs uniquely in neurofibroma SCs (Serra et al., 1997). Neurofibromas may develop from SCs or SCs, because inactivation of *Nf1* at the SCP stage or in adult mice results in neurofibroma formation (Chen et al., 2014; Wu et al., 2008; Zhu et al., 2002). *NF1* encodes the RasGAP protein neurofibromin, and Ras signaling is elevated in neurofibroma SCs (Cichowski and Jaks, 2001). Other genes and signaling pathways that drive neurofibroma initiation and growth are largely unknown.

STAT3 is a latent transcription factor implicated in cancer, which regulates cell-cycle progression and apoptosis. STAT3 phosphorylation at Y705 is essential for STAT3 dimerization, required for STAT3 binding to DNA-promoter regions and transcriptional activation (Battle and Frank, 2002). Fewer benign lesions formed when Stat3 was absent in prostate and skin tumors *in vivo*, implicating it tumor initiation (Kim et al., 2009; Kroon et al., 2013). Stat3 also regulates self-renewal and growth of glioma stem cells (Sherry et al., 2009). Recent studies on MPNST, aggressive nerve sarcomas, implicate Stat3 in their growth (Banerjee et al., 2010; Wu et al., 2014). The role of Stat3 in the benign nerve tumors (neurofibromas) has not been studied.

Stat3 activated β -catenin through GSK3b in hepatocytes (Moh et al., 2008). B-catenin is a developmental signaling pathway re-activated in many cancers. How β -catenin becomes elevated and if β -catenin plays a role in neurofibroma is unknown, although neurofibroma β -catenin expression was reported (Luscan et al., 2014; Mo et al., 2013; Watson et al., 2013). Supporting possible roles for β -catenin in nerve tumorigenesis, *in vivo* activation of β -catenin in developing SCs delays SC differentiation and results in sustained proliferation (Grigoryan et al., 2013).

Multi-subunit SWI/SNF chromatin remodeling complexes modulate transcription factor access to target genes, resulting in activation or repression of transcription (Tolstorukov et al., 2013). Recent studies demonstrate mutation/loss of chromatin remodeling genes in progression to MPNST (De Raedt et al., 2014; Lee et al., 2014), but are unstudied in neurofibromas. Mutational inactivation of SWI/SNF complex genes, including *BRG1/SMARCA4*, encoding a SWI/SNF ATPase, and SWI/SNF subunit genes *ARID1A* and *ARID1B*, are increasingly implicated in development and cancer (Helming et al., 2014; Sausen et al., 2013). When an ARID1B-containing SWI/SNF complex is present, interaction of STAT3 with DNA activates *c-myc* transcription in pre-osteoblast MC3T3-E1 cells (Nagl et al., 2007). Also, BRG1 interacts with β -catenin to promote target-gene activation in colon cancer cells (Barker et al., 2001). In patients with intellectual disability, ARID1B represses *BRG1*-dependent Wnt/ β -catenin signaling (Vasileiou et al., 2015).

We report results of an unbiased *in vivo* Sleeping Beauty insertional mutagenesis transposon screen. We demonstrate a critical role of Stat3 in driving neurofibromas. *Stat3* transcriptionally represses *Gsk3 β* and the SWI/SNF complex subunit *Arid1b*, thereby activating β -catenin in SCs - resulting in neurofibroma initiation and maintenance.

Results

A transposon system and pathway analysis implicate the *Wnt* and *Stat3* pathways in neurofibroma formation

To identify mechanisms underlying neurofibroma growth and/or tumor progression, we used insertional mutagenesis. We generated quadruple transgenic animals (*Nf1^{fl/fl};DhhCre;Rosa26-lsl-SB11;T2/Onc*) (Figure S1A). Survival and onset of tumorigenesis did not differ from control *Nf1^{fl/fl};DhhCre* animals (not shown), and neurofibroma size was similar ($p = 0.1996$) (Figure S1B, upper panel). However, the number of neurofibromas isolated from experimental animals was higher (5.4 vs. 2.8; $p = 0.1017$)

(Figure S1B, lower panel). The trend toward significance in this small sample set suggests that transposition-related genes might play roles in increasing neurofibroma numbers and/or growth.

To identify potential genes responsible for neurofibroma tumorigenesis, we used high-throughput pyrosequencing of neurofibromas isolated from experimental quadruple transgenic animals. We identified 31 common transposon insertion sites (CIS). We removed CISs identified in control insertion-site mapping experiments in 3-week-old transgenic mouse tail DNA carrying both the T2/Onc and *Rosa26-SB11* transgenes, and CISs identified in tumors from single mice. The remaining 22 CISs identified for neurofibroma tumorigenesis are shown in Figure 1A.

We used the Genemania prediction server (<http://www.genemania.org>) to predict pathways, interactions, and functions of the 22 CIS genes, and identified networks including CIS genes. The most significantly deregulated pathways were *Wnt* signaling (FDR=0.021) including CIS genes *Tnks* and *Gsk3 β* , and major neighboring genes: *Strn*, *Axin1*, and *Dvl1*, and *Stat3*-associated cellular carbohydrate metabolic process (FDR=0.023) including the CIS genes *Gsk3 β* and *Arid1b* and major neighboring genes *Stat3* and *Ptpn2* (Figure 1B). Interestingly, *Gsk3 β* connected these two pathways in this in silico analysis. No tumor tissue from these mice was available for confirmatory analysis. The other signaling pathways identified by Genemania are shown in Figure S1C.

STAT3/ β -catenin signaling is activated in mouse and human neurofibromas

We focused on STAT3, a known oncogene and therapeutic target unstudied in neurofibroma. Antibodies recognizing P-Stat3-Y705 detected positive cells in all mouse GEM-neurofibromas (n=19) (Figure 2A), but not wild type mouse sciatic nerves (Figure 2A, insert). In contrast, P-Stat3-Ser727 was detectable in 1/4 mouse and 1/5 human neurofibromas (not shown). Given the link between the Stat and Wnt pathways identified by transposon mutagenesis, we tested if β -catenin is co-activated with P-Stat3 in neurofibroma SCs. *DhhCre* activates EGFP expression in the context of *DhhCreNf1^{fl/fl}* mice in 40–50% of SCs, in a reporter mouse in which the *CMV- β actin* promoter and *loxP* flanked CAT gene are upstream of the *Egfp* cassette (Nakamura et al., 2006). We stained frozen sections of *Nf1^{fl/fl};DhhCre;EGFP* mouse neurofibromas with anti-P-Stat3 and anti- β -catenin. Of EGFP-expressing SCs, 21% were P-Stat3⁺ only, 62% expressed only β -catenin⁺ and, importantly, 6.7% of EGFP⁺ SCs were P-Stat3⁺ and β -catenin⁺ (Figure 2B). Thus, P-Stat3 and β -catenin can be co-activated in SCs in neurofibromas. We also detected Iba1⁺ macrophages that are P-Stat3⁺;EGFP⁻ (not shown). Western blots confirmed robust P-Stat3-Y705 in mouse neurofibroma lysates versus wild-type peripheral nerve (Figure 2C).

We immunolabeled human plexiform neurofibroma sections to test if P-STAT3 and β -catenin expression correlate. Most (29/30) contained P-Y705-STAT3⁺ and β -catenin⁺ cells (Figure 2D–F). Some neurofibroma cells showed cytoplasmic staining (43%), others showed nuclear staining (23%) and 34.2% showed both. There was a significant correlation between P-STAT3 and total β -catenin (Figure 2E, F). Thus, the STAT3 and β -catenin pathways are activated in human neurofibromas, and highly correlated.

Targeted genetic deletion of Stat3 in SCs and SCPs decreases neurofibroma numbers and delays neurofibroma formation in vivo

We then tested if activation of Stat3 in SCs/SCPs is necessary for neurofibroma initiation and/or maintenance. Loss of Stat3 in *Stat3^{fl/fl};DhhCre* mice had no influence on peripheral (saphenous) nerve structure, as shown by electron microscopy; Remak bundles and myelinated axons showed normal differentiated morphology (Figure S2A.S2B). We bred *Stat3^{fl/fl}* mice onto *Nf1^{fl/fl};DhhCre* mice; this required generating recombinants, as both *Nf1* and *Stat3* reside on mouse chromosome 11. Kaplan-Meier survival analysis revealed a significant difference in mouse survival between *Stat3^{fl/fl};Nf1^{fl/fl};DhhCre* mice and *Stat3^{fl/+};Nf1^{fl/fl};DhhCre* mice ($p < 0.001$) or between *Stat3^{fl/fl};Nf1^{fl/fl};DhhCre* mice and *Nf1^{fl/fl};DhhCre* mice ($p < 0.001$). Loss of one Stat3 allele does not influence survival (*Stat3^{fl/+};Nf1^{fl/fl};DhhCre* mice versus *Nf1^{fl/fl};DhhCre* mice $p = 0.66$) (Figure 3A).

Nf1^{fl/fl};DhhCre nerves continually and significantly increased in size, corresponding to neurofibroma initiation and neurofibroma growth reported in this model (Wu et al., 2008). Representative tumors at 9 months are shown in a *Nf1^{fl/fl};DhhCre* versus a *Stat3^{fl/fl};Nf1^{fl/fl};DhhCre* mouse (Figure 3B). We quantified total neurofibroma burden by volumetric measurement of MRI scans, followed by mixed effects analysis of tumor volume. Strikingly, double mutant nerves (average 20mm³) were similar to wild type nerves (8–19 mm³) (Figure 3C). The difference between controls (*Nf1^{fl/fl};DhhCre* or *Stat3^{fl/+};Nf1^{fl/fl};DhhCre*; $n = 9$) and *Stat3^{fl/fl};Nf1^{fl/fl};DhhCre* mice ($n = 15$) was significant ($p < 0.001$ at 4, 7 and 9 months; Figure S2C, S2D).

In the *Nf1^{fl/fl};DhhCre* model each mouse develops 4–20 neurofibromas. If Stat3 contributes to neurofibroma initiation, then tumor number should be reduced in Stat3 mutants. Indeed, *Stat3^{fl/fl};Nf1^{fl/fl};DhhCre* mice had significant fewer tumors/mouse versus *Stat3^{fl/+};Nf1^{fl/fl};DhhCre* littermates at spinal cord dissection at 5 months old mice (Figure 3D). Confirming volumetric MRI scan results, neurofibroma diameter measured at spinal roots on dissection was significantly smaller in *Stat3^{fl/fl};Nf1^{fl/fl};DhhCre* versus *Stat3^{fl/+};Nf1^{fl/fl};DhhCre* mice (Figure 3E). Rare small neurofibromas showed hyperplasia or GEM-grade 1 neurofibroma histology (Figure S3). Ki67⁺ proliferating cells in neurofibroma tissue sections significantly decreased in *Stat3^{fl/fl};Nf1^{fl/fl};DhhCre* neurofibromas (Figure 3F); numbers of dying cells were unchanged (CC3+) (Figure 3G). Importantly, Stat3 protein was absent in flow cytometry-sorted EGFP⁺ SCs and SCPs from *Stat3^{fl/fl};Nf1^{fl/fl};DhhCre,EGFP⁺* mice (Figure 3H); we did, however, detect increased levels of Stat1 and Stat5 (not shown). Therefore, glial cell Stat3 regulates tumor cell proliferation in neurofibromas, and activation of Stat3 in SCs and/or SCPs is important for neurofibroma initiation and growth.

Stat3 contributes to neurofibroma initiation

Our in vivo analyses could not distinguish function(s) of P-Stat3 in neurofibroma SCs versus SCPs, because the genetic loss-of-function targets both. To confirm that Stat3 is relevant to neurofibroma SCP-like cells we used sphere culture, enabling detection of growth and self-renewal of nervous system stem/progenitors. We isolated cells directly from human plexiform neurofibromas and cultured them as floating spheres at clonal density. We

blocked STAT3 signaling with FLLL32, a JAK2/STAT3 inhibitor (Lin et al., 2010). FLLL32 inhibited human neurofibroma sphere formation (IC₅₀ 0.3 μM) (Figure 4A, 4B). Western blot confirmed decreased STAT3-Y705 phosphorylation and slightly reduced total STAT3 (Figure 4C). Importantly, FLLL32 inhibited the formation *Nf1*^{-/-} SCP spheres (IC₅₀ 0.5–1 μM), yet affected wild-type SCPs only at 10x higher concentration (Figure 4D). We also dissociated DRG/early neurofibromas from 6 week old mice. *Stat3^{fl/fl};Nf1^{fl/fl};DhhCre* cells formed significantly fewer primary and secondary spheres than *Nf1^{fl/fl};DhhCre* cells (Figure 4E–F); sphere size was similar (Figure 4E and not shown). We also depleted *Stat3* from *Nf1^{fl/fl};DhhCre* neurofibroma SCP-spheres with shRNAs. Sphere numbers were significantly reduced 4 days after shStat3 infection, versus non-target controls (Figure S4A); we confirmed decreased Stat3 by Western blot (Figure S4B). Thus, Stat3 increases *Nf1* mutant SCP self-renewal. In many cancers, self-renewing stem/progenitor-like cells contribute to tumorigenesis. Neurofibroma like lesions were detected in 7 of 8 *nu/nu* mice that were subcutaneously transplanted with *Nf1^{fl/fl};DhhCre* mice derived sphere cells (Figure 4G, 4H), while no lesion was detected in *Stat3^{fl/fl};Nf1^{fl/fl};DhhCre* derived sphere cells (Figure 4G). Hematoxylin and eosin staining of tissue sections showed no features of malignancy (Figure 4I), and anti-S100β⁺ cells SCs (Figure 4J) and mast cells (Figure 4K). On EM, these lesions contained SCs identified by their continuous basal lamina and wrapping of small axons (Figure 4L), blood vessels (Figure 4M) and mast cells (Figure 4N)—all features of neurofibroma. These in vitro and in vivo genetic results support the conclusion that *Nf1*^{-/-} SCP self-renewal and neurofibroma tumorigenic potential are regulated by Stat3.

Stat3 activates β-catenin signaling

Data in Figures 1 and 2 suggest a Stat3-β-catenin link in neurofibroma SCs. Stabilized β-catenin translocates to the nucleus and alters target gene transcription (Liu et al., 2002). *Stat3^{fl/fl};Nf1^{fl/fl};DhhCre* neurofibromas showed significantly decreased active (nuclear) β-catenin (45%), increased inactive β-catenin (P-β-catenin, S33, S37, and T41) (591% in cytoplasm, 166% in nucleus) and decreased cyclin D1 expression (>90% in cytoplasm and nucleus versus controls (Figure 5A). In contrast, P-Erk did not change (Figure 5A). Thus, neurofibroma β-catenin expression, localization, and target gene expression are regulated by Stat3.

To verify this conclusion in a system amenable for mechanistic analysis, we isolated SCPs from *Nf1^{fl/fl};DhhCre* neurofibromas and cultured them with or without blocking β-catenin signaling with the tankyrase inhibitor XAV-939, which stabilizes axin, a component of the β-catenin destruction complex. XAV-939 inhibited mouse neurofibroma sphere formation (IC₅₀ 0.1 μM). Western blot confirmed a 50% decrease in total β-catenin with 3 days of drug exposure (10nM) (Figure 5B). Supporting the hypothesis that Stat3 is critical for β-catenin expression, remarkably, *Stat3^{fl/fl};Nf1^{fl/fl};DhhCre* mouse neurofibroma spheres were insensitive to 100X higher concentrations of XAV-939 (Figure 5C). Depleting β-catenin with shRNAs in *Nf1^{fl/fl};DhhCre* neurofibroma SCP-like spheres also significantly reduced sphere numbers versus controls (Figure 5D); we confirmed decreased β-catenin by Western blot (Figure 5D insert). Thus β-catenin stabilization requires Stat3 in *Nf1*^{-/-} neurofibroma derived SCP-like cells.

If β -catenin is critical in Stat3-driven neurofibromagenesis, then *Stat3^{fl/fl};Nf1^{fl/fl};DhhCre* spheres, which do not form tumors, should be rescued by β -catenin. To test this, we infected spheres with a stable, active, β -catenin mutant (N90 β -cat) or virus control. Remarkably, overexpression of N90 β -catenin significantly increased the number of *Stat3^{fl/fl};Nf1^{fl/fl};DhhCre*, but not *Nf1^{fl/fl};DhhCre*, neurofibroma spheres (Figure 5E). Importantly, 7/9 mice injected with N90 β -catenin infected *Stat3^{fl/fl};Nf1^{fl/fl};DhhCre* spheres developed neurofibroma like lesions, while no lesions were detected in vector controls. Thus β -catenin is a major effector of Stat3 signaling in SCP, and necessary for neurofibromagenesis.

Stat3 alters Gsk3 β inhibitory phosphorylation

We wondered how Stat3 activates β -catenin in neurofibromas. *Gsk3 β* was a frequent CIS identified in our insertional mutagenesis screen, which predicted reduced GSK3 β (Figure 1). GSK3 β (Ser9) phosphorylation inhibits GSK3 β activity, allowing β -catenin stabilization/activation (Wu and Pan, 2010). *STAT3* can negatively regulate *GSK3 β* transcription (Moh et al., 2008). Supporting the idea that Stat3 transcriptionally represses *Gsk3 β* in neurofibromas, *Gsk3 β* mRNA expression increased in *Stat3^{fl/fl};Nf1^{fl/fl};DhhCre* versus *Nf1^{fl/fl};DhhCre* neurofibromas (Figure S5A). ChIP using anti-Stat3 detected Stat3 bound to the Stat3 binding motif in the *Gsk3 β* 5' UTR in neurofibroma DNA (Figure S5B, S5C). Furthermore, in the absence of Stat3 total *Gsk3 β* increased in neurofibromas (Figure S5D). Thus, in neurofibromas Stat3 represses *Gsk3 β* transcription, correlating with a reduction in *Gsk3 β* protein. However, targeting *Gsk3 β* with shRNA did not significantly rescue sphere formation in *Stat3^{fl/fl};Nf1^{fl/fl};DhhCre* SCP spheres (Figure S5E), suggesting the existence of additional pathways.

Stat3 transcriptionally represses *Arid1b* expression

Arid1b was another frequent CIS identified by insertional mutagenesis (Figure 1A). Transposon insertions into the *Arid1b* locus predicted disrupted C-termini or truncated N-termini, e.g. inactivating insertions, and anti-*Arid1b* immunofluorescence was strong in WT SCs but reduced in neurofibroma SCs (Figure S6A). QRT-PCR confirmed negative regulation of *Arid1b* mRNA expression in neurofibromas by Stat3 (e.g. *Arid1b* mRNA is low in neurofibroma and increases in the absence of *Stat3*; Figure 6A). Similar results were observed in FACS-sorted EGFP⁺ neurofibroma SCs vs WT SCs (Figure S6B). We identified a putative Stat3 binding site 7kb downstream of the mouse *Arid1b* transcriptional start site (Figure 6B and Figure S7). When *Nf1^{fl/fl};DhhCre* neurofibroma DNA was subjected to ChIP using anti-Stat3, we detected Stat3 bound to *Arid1b* at this site by PCR (Figure 6C).

Arid1b expression was low in *Nf1^{fl/fl};DhhCre* and high in *Stat3^{fl/fl};Nf1^{fl/fl};DhhCre* tumor-derived neurofibroma spheres (not shown). We exposed *Stat3^{fl/fl};Nf1^{fl/fl};DhhCre* neurofibroma spheres to sh*Arid1b*. Decreasing *Arid1b* expression significantly increased sphere numbers (Figure 6D), correlating with elevated levels of activated β -catenin protein (Figure 6E) and mRNA expression (Figure 6G), and elevated levels of the β -catenin target genes *Axin2*, *Ccnd1*, and *Myc* (Figure 6G). *ShGsk3 β* increased β -catenin and its target gene mRNA expression in *Stat3^{fl/fl};Nf1^{fl/fl};DhhCre* spheres (Figure 6F), but did not rescue numbers of *Stat3^{fl/fl};Nf1^{fl/fl};DhhCre* spheres (Figure S5E, Figure 7B). Knockdown of *Gsk3 β*

and *Arid1b* simultaneously with shRNA showed similar effects to *shArid1b* alone (Figure 7A).

To test whether tumor formation is affected by reduction in *Arid1b*, *Gsk3 β* , or both, we transplanted sphere cells into nude mice. *Stat3^{fl/fl};Nf1^{fl/fl};DhhCre* spheres rarely formed tumors. Tumors formed in *Stat3^{fl/fl};Nf1^{fl/fl};DhhCre* sphere cells infected with sh*Gsk3 β* , sh*Arid1b* or sh*Arid1b* + sh*Gsk3 β* by 8 weeks after transplantation ($p=0.0157$; Figure 7B). There were no significant differences between the three experimental groups ($p=0.3669$), suggesting both *Gsk3 β* and *Arid1b* are involved in *Stat3*-mediated neurofibromagenesis.

ARID1B acts in SWI/SNF complexes containing BRG1, the central catalytic subunit of numerous chromatin-modifying enzymatic complexes (Trotter and Archer, 2008). BRG1 can be required for Stat3 recruitment to target genes (Ni and Bremner, 2007). To test whether *Arid1b* requires Brg1 to affect sphere numbers, we knocked down *Brg1* and/or *Arid1b* in *Stat3^{fl/fl};Nf1^{fl/fl};DhhCre* spheres with shRNA. The low numbers characteristic of *Stat3^{fl/fl};Nf1^{fl/fl};DhhCre* spheres were rescued by *shArid1b*, but not sh*Brg1*. The combination of *shArid1b* together with sh*Brg1* prevented the *shArid1b* effect, indicating that the effect requires Brg1 and likely chromatin remodeling (Figure 7C).

Stat3 binds the *Arid1b* promoter fragment, repressing *Arid1b* expression. *Arid1b*'s known function is in chromatin remodeling, and we wondered if the *Arid1b* gene itself might be subject to Stat3-dependent histone modification. We performed CHIP with antibodies recognizing the histone modifications H3K4Me₃, H3K9Me₂, and H3K9Ac in vehicle or Stat3 inhibitor (FLLL32) treated primary mouse neurofibroma SCs at the *Arid1b* promoter. We detected a significant enhancement in the H3K4Me₃ marks at the *Arid1b* promoter in three independent experiments ($p<0.05$). In contrast, H3K9Me₂ or H3K9Ac did not significantly change at this site after FLLL32 exposure (Figure 7D). Taken together, in the setting of *Nf1* loss, Stat3 transcriptionally represses the SWI/SNF gene *Arid1b* through histone H3K4Me₃ modification and this repression is BRG1 dependent (Figure 7E). This results in an increase in β -catenin.

Discussion

Through performing an unbiased insertional mutagenesis screen, use of mouse genetics and SCP culture we identified an *Nf1*/P-Stat3/*Arid1b*/ β -catenin pathway in SCP that is critical for neurofibroma initiation. P-Stat3 is a major neurofibroma oncogene as targeted genetic deletion of *Stat3* in nerve SCs and SCPs dramatically delays neurofibroma formation and tumors, once formed, grow very slowly (Figure 2A–C). *Stat3* provides a first example of a genetic loss of function affecting neurofibroma initiation and growth in vivo. Loss of *Stat3* decreased numbers of neurofibroma SCP-like cells, neurofibroma SCP self-renewal, and neurofibroma formation by SCP after transplantation, functions defining cancer stem/progenitor-like cells in tumor initiation (Figure 4). Importantly, β -catenin expression rescued all Stat3-loss of function driven phenotypes in *Nf1* mutant SCPs (Figure 5E). Supporting the relevance of our findings to human neurofibroma, primary patient-derived neurofibroma SCP-like cell sphere formation, a surrogate of tumor initiation, was dramatically reduced by

Jak2/Stat3 inhibition (Figure 4A), and P-Y705-STAT3 and β -catenin expression were highly correlated in human plexiform neurofibromas (Figure 2).

We confirmed that Stat3 and β -catenin are detectable in human plexiform neurofibroma, and demonstrated that Stat3 and β -catenin are critical for neurofibroma formation in transplantation (Figure 5G). The Sleeping Beauty system and pathway analysis defined mutations predicting loss of *Gsk3 β* and *Arid1b*, identifying the *WNT* and *STAT* pathways as players that might cooperate with loss of *Nf1* in neurofibromagenesis (Figure 1). *GSK3 β* and β -catenin signaling were previously implicated in MPNST, sarcomas that are malignant derivatives of neurofibromas (Mo et al., 2013; Rahrman et al., 2013; Watson et al., 2013). Other CIS genes (*WAPAL*, *SP3*, *BTBD9*, and *IGFR1*) are up-regulated in neurofibroma cells, suggesting roles as proto-oncogenes early in tumor progression. Down-regulated CIS genes (*TMCC3*, *SLC35F1*, and *SORCS*) may have tumor suppressor functions.

Stat3 is present on the *Gsk3 β* promoter in neurofibromas (Figure S5), consistent with Stat3 repressing *GSK3 β* transcription in hepatocytes (Moh et al., 2008). In SCP, decreasing *Gsk3 β* also increased β -catenin target gene expression, and tumor formation, but did not rescue SCP sphere formation. Given that sh*Gsk3 β* or sh*Arid1b* enable tumor formation and β -catenin expression, but only sh*Arid1b* rescues neurofibroma sphere number, these genes likely use different mechanisms to repress β -catenin function; loss of either is sufficient to drive neurofibroma formation in the absence of Stat3, suggesting that interference with β -catenin signaling by one of several mechanisms will interfere with tumor formation.

We identify *Arid1b* as a critical link between P-Stat3 and β -catenin. *ARID1B* is a tumor suppressor, mutated by deletion, in neuroblastoma (Sausen et al., 2013). The *ARID1B* promoter can be hyper-methylated, resulting in decreased *ARID1B* expression, as in pancreatic cancer cells (Khurshed et al., 2013). *Arid1b* also functions as a tumor suppressor in the context of *Nf1* loss, with low expression in neurofibromas resulting in increased β -catenin, Wnt/ β -catenin target gene expression, and tumorigenesis (Figure 6). There was variation in the extent of Wnt/ β -catenin target gene expression among samples on shRNA exposure, which is likely due to our use of primary cells. The differentiation state of individual cells in spheres and/or different levels of shRNA expression after lentiviral infection may account for this variation. While our study was nearing completion, Vasileiou et al. (2015) showed that, as in our study, reducing *ARID1B* increases Wnt/ β -catenin target gene expression. They also overexpressed *ARID1B* by transient transfection and inhibited Wnt/ β -catenin activity in cell lines. We were unable to overexpress *ARID1B*, as the *ARID1B* cDNA is too large for the lentiviral infection required in our primary cells. Nevertheless, together the two studies strongly support critical roles for *ARID1B* in regulation of Wnt/ β -catenin activity.

We detected increased H3K4Me₃ at the *Arid1b* promoter region after Stat3 inhibition. Given that the Stat3 binding site is in intron 1 of the *Arid1b* gene, it is likely that Stat3 binds to this intronic region and regulates *Arid1b* by antisense transcription, a mechanism by which mammalian genes regulate sense transcription (Faghihi and Wahlestedt, 2009; Magistri et al., 2012). Genome-wide mapping of chromatin modification will be necessary to further clarify this mechanism.

In summary, loss of *Nf1* activates Stat3 SCPs, enabling tumor initiation by repressing the SWI/SNF gene *Arid1b* through histones H3K4Me3 and H3K27Me3 modification, thereby activating β -catenin. Knock-down of *Arid1b* in *Stat3^{fl/f};Nf1^{fl/fl};DhhCre* SCPs by shRNA is sufficient to rescue neurofibroma formation in in vivo transplantation. Mouse and human *NF1* mutant cells are significantly more sensitive than their wild type counterparts to treatment with a JAK2/STAT3 inhibitor (Figure 4A, 4D), suggesting that a therapeutic window will exist for neurofibroma therapy using JAK/STAT pathway inhibitors now in clinical trials (Lesina et al., 2011). Given that β -catenin targeted therapeutics are not yet proven, blocking β -catenin via STAT or targeting SWI/SNF complexes may be feasible strategies.

Experimental Procedures

Animals

Mice were housed in temperature- and humidity-controlled facilities on 12-hour dark-light cycles with free access to food and water. The animal care and use committees of Cincinnati Children's Hospital Medical Center or University of Minnesota approved all animal procedures. See Supplemental Experimental Procedures for additional details.

Pyrosequencing and Genemania analysis

T2/Onc integration sites from 49 neurofibromas were cloned and sequenced using bar-coded primers and linker-mediated PCR, followed by pyrosequencing. Amplicon sequencing using the GS20 Flex pyrosequencing machine (Roche, Indianapolis, IN) was performed according to the manufacturer's protocol. Primers used a unique 10-bp barcode-recognition sequence for each tumor sample. After removal of redundant and other non-specific noise as described (Keng et al., 2009), we obtained 6,353 non-redundant insertions. Next, we identified CISs with more Sleeping Beauty mutagenic transposon insertions than predicted based on Monte Carlo criteria for statistical significance. We defined CISs as regions in the genome with six insertions located within 185 kb of each other, five insertions within 95 kb, four insertions within 35 kb, or three insertions within 5 kb. We used the Genemania algorithm to generate gene-gene association networks (genetic interaction, physical interaction, and pathways), after inputting these CIS. This generated networks, each of which we extended using the top 20 related genes precomputed in the program. These are defined as neighboring genes. We similarly colored genes significantly enriched in a given "biological process" within a Gene-Ontology (GO) category, after applying a significance cutoff of $FDR < 0.05$.

Embryonic and Neurofibroma sphere formation and SC culture

Embryonic mouse spheres, dissociated from E12.5 DRG with 0.25% Trypsin 20 min. at 37°C (Mediatech; Herndon, VA) produced single-cell suspensions with narrow-bore pipettes and a 70 μ m strainer (BD-Falcon). For mouse or human neurofibroma spheres, we chopped tissue into 1–3 mm³ pieces, plated in 20mL L-15 (Mediatech) plus 0.5 mg/mL collagenase type 1 (Worthington; Lakewood, NJ), and 2.5 mg/mL dispase protease type II (Cambrex; East Rutherford, NJ) at 37°C for 4–6 hours. We plated trypan blue negative cells (Stem Cell Technologies, Vancouver, BC) at 1×10^4 cells in 1 mL per well in 24-well low-binding plates in medium containing DMEM:F-12 (3:1) + 20 ng/ml rhEGF (R&D Systems), 20

ng/ml rh bFGF (R&D Systems), 1% B-27 (Invitrogen), 2 µg/ml heparin (Sigma). We maintained cultures at 37°C and 5% CO₂ and counted floating spheres after 4–7 days. To passage, we centrifuged sphere cultures, dissociated and plated at 1 × 10⁴ cells/ml in fresh sphere medium as described (Williams et al., 2008). For each experiment, we show a representative of 3 independent experiments.

Immunohistochemistry

Tissue was embedded in paraffin, and 6-µm sections were cut and stained with either H&E, toluidine blue or incubated overnight at 4°C with antibody: anti-S100β, Dako, Carpinteria, CA), Ki67 (Novacastra Leica Microsystems, Buffalo Grove, IL) or anti-P-Stat3 (Y705), anti-cleaved caspase 3, β-catenin (Cell Signaling, Danvers, MA). Visualization methods were as described (Williams et al., 2008).

Western blots

Western blots were performed using antibodies recognizing P-Jak2, Jak2, P-Stat3, Stat3, P-β-catenin, β-catenin, P-GSK3β, GSK3β, and β-actin (Cell Signaling, MA). At least three different tumor/cell lysates were analyzed per antigen.

Tumorigenesis assay in nude mice

We injected 5×10⁵ mouse sphere cells/injection subcutaneously into athymic female nude mice (Harlan, Indianapolis, IN). After two months we dissected tumors and fixed them in 4% paraformaldehyde overnight, then embedded in paraffin for histology.

Measurement of tumor number and tumor size

We perfused each mouse intracardially with 4% paraformaldehyde (w/v) in PBS, incubated overnight in 300 ml 4% paraformaldehyde, incubated overnight, again, in 50 ml decalcification solution (Cal-Rite, Richard Allan Scientific, Kalamazoo, MI), and then transferred to PBS. Using a Leica dissecting microscope, we dissected the spinal cord with attached DRG and nerve roots, and counted tumors. A tumor was defined as a mass surrounding the DRG and/or nerve roots, with a diameter greater than 1 mm, measured perpendicular to DRG/nerve roots.

Tumor volumetric measurement

MRI imaging and volumetric measurement of neurofibromas and statistical analyses using mixed effects modeling were as described (Wu et al., 2012).

Lentiviral infection

We infected secondary *Nf1^{fl/fl};DhhCre* neurofibroma spheres or *Stat3^{fl/fl};Nf1^{fl/fl};DhhCre* DRG/neurofibroma spheres with shRNAs and non-target control (Sigma, St Louis, MO, USA), β-catenin overexpression lentivirus N90 (Addgene, Cambridge MA) or same backbone control (Sigma). We incubated lentiviral particles with neurofibroma spheres for 3–5 days and counted sphere numbers. For in vivo xenografts, *Stat3^{fl/fl};Nf1^{fl/fl};DhhCre* DRG/neurofibroma spheres were infected with lentivirus in the presence of polybrene (8

µg/ml; Sigma-Aldrich) for 16–20 hours, followed by selection in G418 (500mg/ml; Sigma-Aldrich). Spheres were collected and dissociated for xenograft injection.

Statistics

Kaplan Meier analysis used a Gehan-Breslow-Wilcox log-rank test. Neurofibroma growth was modeled by Mixed Effects Model Analysis. *P* values were generated with a random effects model analysis on log transformed tumor volume data using the SAS mixed procedure (Jessen et al., 2013). We used unpaired 2-tailed Student's *t* tests to analyze significance of cell proliferation and cell death quantification in tissue sections when two samples were compared. Other experiments used Ordinary one way ANOVA, reported as mean ± SEM. *P*<0.05 was considered significant.

Supplementary Material

Refer to Web version on PubMed Central for supplementary material.

Acknowledgments

We thank the Minnesota Supercomputing Institute for computational resources for sequence analysis, Dr. Ari Melnick (Weil Cornell Medical School) for assistance in design of histone modification analysis, and Ms. Huiqing Li for animal husbandry. This work was supported by NIH R01 NS28840 (N.R.), NIH P50 NS057531 (N.R. and D.L.), a DAMD New Investigator Award (W81XWH-11-1-0259) and an Ohio State University Comprehensive Cancer Center Pelotonia Idea Grant (J.W.), and the American Cancer Society (IRG-67-003-44) (J.R.F.). The CHTN provided some benign neurofibromas used in this study (IRB approved).

References

- Banerjee S, Byrd JN, Gianino SM, Harpstrite SE, Rodriguez FJ, Tuskan RG, Reilly KM, Piwnicka-Worms DR, Gutmann DH. The neurofibromatosis type 1 tumor suppressor controls cell growth by regulating signal transducer and activator of transcription-3 activity in vitro and in vivo. *Cancer Res.* 2010; 70:1356–1366. [PubMed: 20124472]
- Barker N, Hurlstone A, Musisi H, Miles A, Bienz M, Clevers H. The chromatin remodelling factor Brg-1 interacts with beta-catenin to promote target gene activation. *EMBO J.* 2001; 20:4935–4943. [PubMed: 11532957]
- Battle TE, Frank DA. The role of STATs in apoptosis. *Curr Mol Med.* 2002; 2:381–392. [PubMed: 12108949]
- Boyd KP, Korf BR, Theos A. Neurofibromatosis type 1. *J Am Acad Dermatol.* 2009; 61:1–14. [PubMed: 19539839]
- Chen Z, Liu C, Patel AJ, Liao CP, Wang Y, Le LQ. Cells of origin in the embryonic nerve roots for NF1-associated plexiform neurofibroma. *Cancer Cell.* 2014; 26:695–706. [PubMed: 25446898]
- Cichowski K, Jacks T. NF1 tumor suppressor function: narrowing the GAP. *Cell.* 2001; 104:593–604. [PubMed: 11239415]
- De Raedt T, Beert E, Pasmant E, Luscan A, Brems H, Ortonne N, Helin K, Hornick JL, Mautner V, Kehrer-Sawatzki H, et al. PRC2 loss amplifies Ras-driven transcription and confers sensitivity to BRD4-based therapies. *Nature.* 2014; 514:247–251. [PubMed: 25119042]
- Faghihi MA, Wahlestedt C. Regulatory roles of natural antisense transcripts. *Nat Rev Mol Cell Biol.* 2009; 10:637–643. [PubMed: 19638999]
- Grigoryan T, Stein S, Qi J, Wende H, Garratt AN, Nave KA, Birchmeier C, Birchmeier W. Wnt/ Rspodin/beta-catenin signals control axonal sorting and lineage progression in Schwann cell development. *Proc Natl Acad Sci U S A.* 2013; 110:18174–18179. [PubMed: 24151333]

- Helming KC, Wang X, Wilson BG, Vazquez F, Haswell JR, Manchester HE, Kim Y, Kryukov GV, Ghandi M, Aguirre AJ, et al. ARID1B is a specific vulnerability in ARID1A-mutant cancers. *Nat Med.* 2014; 20:251–254. [PubMed: 24562383]
- Jessen WJ, Miller SJ, Jousma E, Wu J, Rizvi TA, Brundage ME, Eaves D, Widemann B, Kim MO, Dombi E, et al. MEK inhibition exhibits efficacy in human and mouse neurofibromatosis tumors. *J Clin Invest.* 2013; 123:340–347. [PubMed: 23221341]
- Keng VW, Villanueva A, Chiang DY, Dupuy AJ, Ryan BJ, Matise I, Silverstein KA, Sarver A, Starr TK, Akagi K, et al. A conditional transposon-based insertional mutagenesis screen for genes associated with mouse hepatocellular carcinoma. *Nat Biotech.* 2009; 27:264–274.
- Khurshid M, Kolla JN, Kotapalli V, Gupta N, Gowrishankar S, Uppin SG, Sastry RA, Koganti S, Sundaram C, Pollack JR, Bashyam MD. ARID1B, a member of the human SWI/SNF chromatin remodeling complex, exhibits tumour-suppressor activities in pancreatic cancer cell lines. *Br J Cancer.* 2013; 108:2056–2062. [PubMed: 23660946]
- Kim DJ, Kataoka K, Rao D, Kiguchi K, Cotsarelis G, Digiovanni J. Targeted disruption of stat3 reveals a major role for follicular stem cells in skin tumor initiation. *Cancer Res.* 2009; 69:7587–7594. [PubMed: 19738054]
- Kroon P, Berry PA, Stower MJ, Rodrigues G, Mann VM, Simms M, Bhasin D, Chettiar S, Li C, Li PK, et al. JAK-STAT blockade inhibits tumor initiation and clonogenic recovery of prostate cancer stem-like cells. *Cancer Res.* 2013; 73:5288–5298. [PubMed: 23824741]
- Lee W, Teckie S, Wiesner T, Ran L, Prieto Granada CN, Lin M, Zhu S, Cao Z, Liang Y, Sboner A, et al. PRC2 is recurrently inactivated through EED or SUZ12 loss in malignant peripheral nerve sheath tumors. *Nat Genet.* 2014; 46:1227–1232. [PubMed: 25240281]
- Lesina M, Kurkowski M, Ludes K, Rose-John S, Treiber M, Klöppel G, Yoshimura A, Reindl W, Sipos B, Akira S, et al. Stat3/Socs3 activation by IL-6 transsignaling promotes progression of pancreatic intraepithelial neoplasia and development of pancreatic cancer. *Cancer Cell.* 2011; 19:456–469. [PubMed: 21481788]
- Lin L, Hutzen B, Zuo M, Ball S, Deangelis S, Foust E, Pandit B, Ihnat M, Shenoy S, Kulp S, et al. Novel STAT3 phosphorylation inhibitors exhibit potent growth-suppressive activity in pancreatic and breast cancer cells. *Cancer Res.* 2010; 70:2445–2454. [PubMed: 20215512]
- Liu C, Li Y, Semenov M, Han C, Baeg GH, Tan Y, Zhang Z, Lin X, He X. Control of beta-catenin phosphorylation/degradation by a dual-kinase mechanism. *Cell.* 2002; 108:837–847. [PubMed: 11955436]
- Luscan A, Shackelford G, Masliah-Planchon J, Laurendeau I, Ortonne N, Varin J, Lallemand F, Leroy K, Dumaine V, Hivelin M, et al. The Activation of the WNT Signaling Pathway Is a Hallmark in Neurofibromatosis Type 1 Tumorigenesis. *Clin Cancer Res.* 2014; 20:358–371. [PubMed: 24218515]
- Magistri M, Faghihi MA, St Laurent G 3rd, Wahlestedt C. Regulation of chromatin structure by long noncoding RNAs: focus on natural antisense transcripts. *Trends Genet.* 2012; 28:389–396. [PubMed: 22541732]
- Mo W, Chen J, Patel A, Zhang L, Chau V, Li Y, Cho W, Lim K, Xu J, Lazar AJ, et al. CXCR4/CXCL12 mediate autocrine cell-cycle progression in NF1-associated malignant peripheral nerve sheath tumors. *Cell.* 2013; 152:1077–1090. [PubMed: 23434321]
- Moh A, Zhang W, Yu S, Wang J, Xu X, Li J, Fu XY. STAT3 sensitizes insulin signaling by negatively regulating glycogen synthase kinase-3 beta. *Diabetes.* 2008; 57:1227–1235. [PubMed: 18268048]
- Nagl NG Jr, Wang X, Patsialou A, Van Scoy M, Moran E. Distinct mammalian SWI/SNF chromatin remodeling complexes with opposing roles in cell-cycle control. *EMBO J.* 2007; 26:752–763. [PubMed: 17255939]
- Nakamura T, Colbert M, Robbins J. Neural crest cells retain multipotential characteristics in the developing valves and label the cardiac conduction system. *Circ Res.* 2006; 98:1547–1554. [PubMed: 16709902]
- Ni Z, Bremner R. Brahma-related gene 1-dependent STAT3 recruitment at IL-6-inducible genes. *J Immunol.* 2007; 178:345–351. [PubMed: 17182572]
- Rahrmann EP, Watson AL, Keng VW, Choi K, Moriarity BS, Beckmann DA, Wolf NK, Sarver A, Collins MH, Moertel CL, et al. Forward genetic screen for malignant peripheral nerve sheath

- tumor formation identifies new genes and pathways driving tumorigenesis. *Nat Genet.* 2013; 45:756–766. [PubMed: 23685747]
- Sausen M, Leary RJ, Jones S, Wu J, Reynolds CP, Liu X, Blackford A, Parmigiani G, Diaz LA Jr, Papadopoulos N, et al. Integrated genomic analyses identify ARID1A and ARID1B alterations in the childhood cancer neuroblastoma. *Nat Genet.* 2013; 45:12–17. [PubMed: 23202128]
- Serra E, Puig S, Otero D, Gaona A, Kruyer H, Ars E, Estivill X, Lázaro C. Confirmation of a double-hit model for the NF1 gene in benign neurofibromas. *Am J Hum Genet.* 1997; 61:512–519. [PubMed: 9326316]
- Sherry MM, Reeves A, Wu JK, Cochran BH. STAT3 is required for proliferation and maintenance of multipotency in glioblastoma stem cells. *Stem Cells.* 2009; 27:2383–2392. [PubMed: 19658181]
- Tolstorukov MY, Sansam CG, Lu P, Koellhoffer EC, Helming KC, Alver BH, Tillman EJ, Evans JA, Wilson BG, Park PJ, Roberts CW. Swi/Snf chromatin remodeling/tumor suppressor complex establishes nucleosome occupancy at target promoters. *Proc Natl Acad Sci U S A.* 2013; 110:10165–10170. [PubMed: 23723349]
- Trotter KW, Archer TK. The BRG1 transcriptional coregulator. *Nucl Recept Signal.* 2008; 6:e004. [PubMed: 18301784]
- Vasileiou G, Ekici AB, Uebe S, Zweier C, Hoyer J, Engels H, Behrens J, Reis A, Hadjihannas MV. Chromatin-Remodeling-Factor ARID1B Represses Wnt/beta-Catenin Signaling. *Am J Hum Genet.* 2015; 97:445–456. [PubMed: 26340334]
- Watson AL, Rahrman EP, Moriarity BS, Choi K, Conboy CB, Greeley AD, Halfond AL, Anderson LK, Wahl BR, Keng VW, et al. Canonical Wnt/beta-catenin signaling drives human schwann cell transformation, progression, and tumor maintenance. *Cancer Discov.* 2013; 3:674–689. [PubMed: 23535903]
- Williams JP, Wu J, Johansson G, Rizvi TA, Miller SC, Geiger H, Malik P, Li W, Mukoyama YS, Cancelas JA, Ratner N. Nf1 mutation expands an EGFR-dependent peripheral nerve progenitor that confers neurofibroma tumorigenic potential. *Cell Stem Cell.* 2008; 3:658–669. [PubMed: 19041782]
- Wu D, Pan W. GSK3: a multifaceted kinase in Wnt signaling. *Trends in biochemical sciences.* 2010; 35:161–168. [PubMed: 19884009]
- Wu J, Dombi E, Jousma E, Scott Dunn R, Lindquist D, Schnell BM, Kim MO, Kim A, Widemann BC, Cripe TP, Ratner N. Preclinical testing of sorafenib and RAD001 in the Nf1(flox/flox); DhhCre mouse model of plexiform neurofibroma using magnetic resonance imaging. *Pediatr Blood Cancer.* 2012; 58:173–180. [PubMed: 21319287]
- Wu J, Patmore DM, Jousma E, Eaves DW, Breving K, Patel AV, Schwartz EB, Fuchs JR, Cripe TP, Stemmer-Rachamimov AO, Ratner N. EGFR-STAT3 signaling promotes formation of malignant peripheral nerve sheath tumors. *Oncogene.* 2014; 33:173–180. [PubMed: 23318430]
- Wu J, Williams JP, Rizvi TA, Kordich JJ, Witte D, Meijer D, Stemmer-Rachamimov AO, Cancelas JA, Ratner N. Plexiform and dermal neurofibromas and pigmentation are caused by Nf1 loss in desert hedgehog-expressing cells. *Cancer Cell.* 2008; 13:105–116. [PubMed: 18242511]
- Zhu Y, Ghosh P, Charnay P, Burns D, Parada L. Neurofibromas in NF1: Schwann cell origin and role of tumor environment. *Science.* 2002; 296:920–922. [PubMed: 11988578]

Highlights

1. Insertional mutagenesis identifies *STAT3* as a driver of benign neurofibroma.
2. Stat3 activates β -catenin to initiate neurofibroma formation.
3. Stat3 represses *Gsk3 β* and *Arid1b* to increase beta-catenin.
4. Neurofibroma-initiating cells require Stat3 and β -catenin for tumorigenesis.

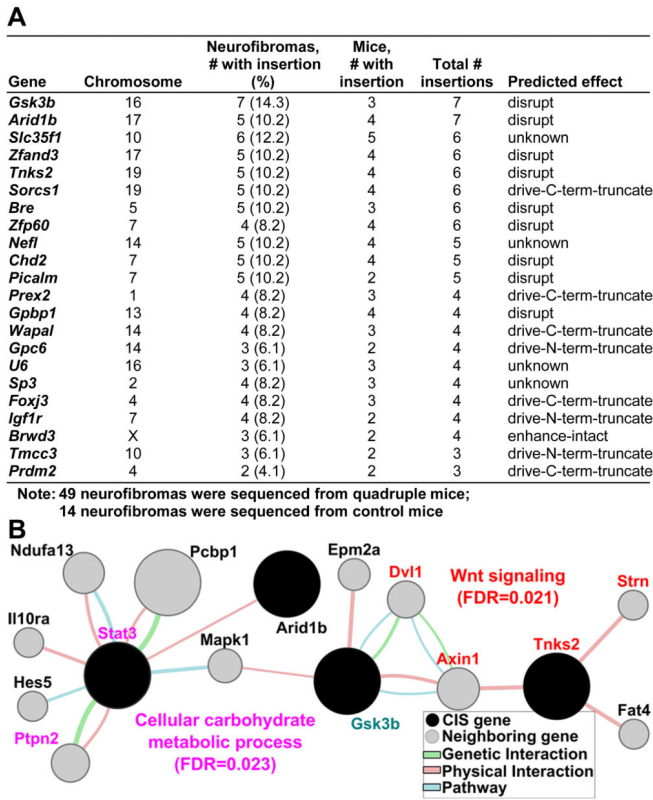


Figure 1. Genes identified by Sleeping Beauty Transposon System predict *STAT3* and *WNT* pathway activation in neurofibroma

(A) Common insertion sites (CIS) identified from neurofibromas. The positions were based on the Ensembl NCBI m37 April 2007 mouse assembly. (B) Genemania pathway analysis using 22 CIS (black) and 20 genes (grey) connected to CIS by genetic, physical or pathway analysis identifies two significantly deregulated networks. WNT signaling related gene names are shown in Red and Cellular carbohydrate metabolic process related genes are in pink. GSK3b (turquoise) connects these pathways to those in Supplemental Figure 2. Circle size correlates to network association probabilities.

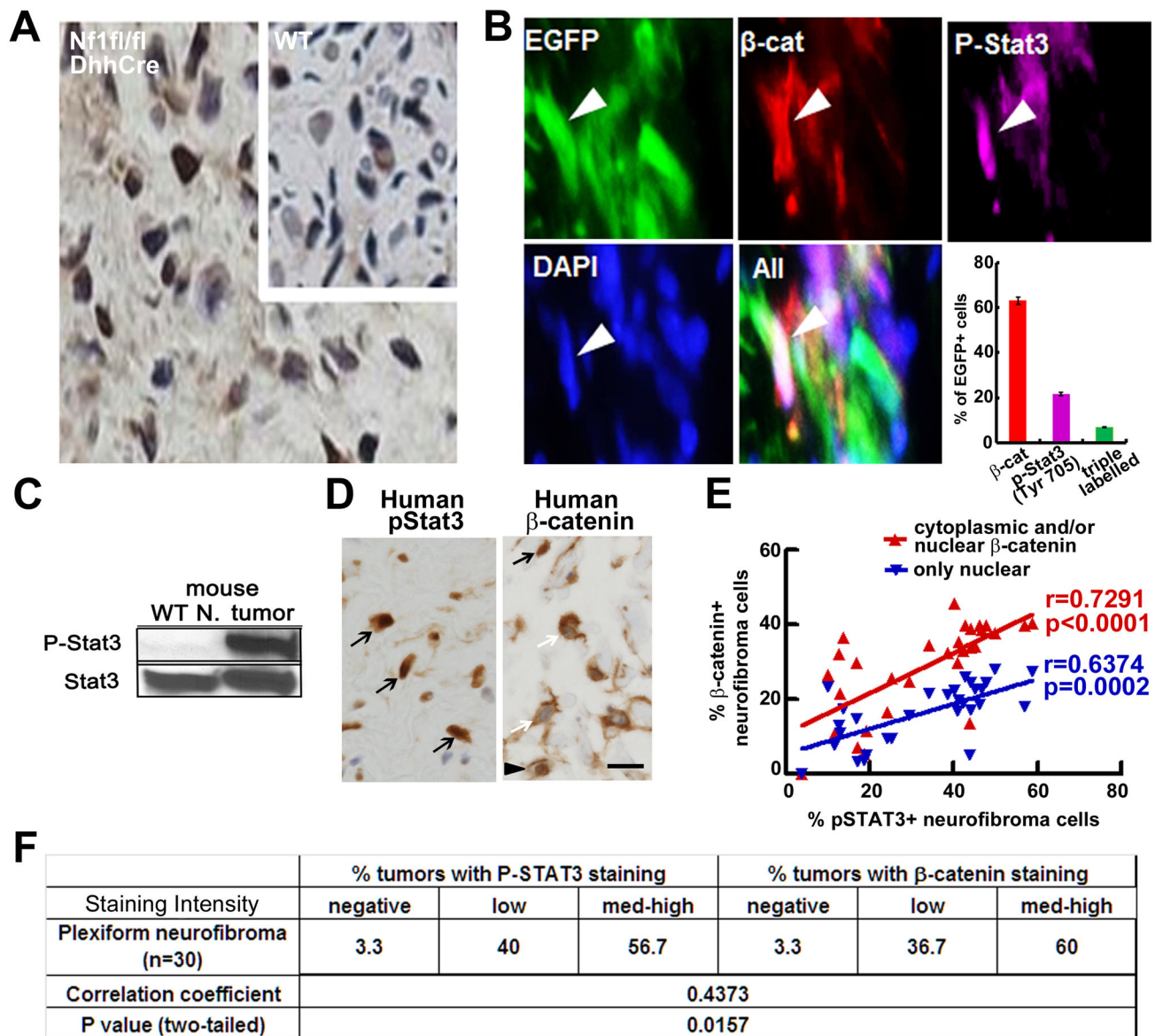


Figure 2. P-STAT3 and β -catenin expression correlate in mouse and human neurofibromas
(A) P-Stat3 immunostaining in mouse neurofibromas and wild type sciatic nerves (insert), visualized with DAB (brown). Nuclei are counterstained with hematoxylin (blue). **(B)** Representative immunofluorescent images show EGFP⁺ SCs (white arrows); some are also P-Stat3⁺ (purple) and β -catenin⁺ (red). Neurofibromas from 3 mice (4 sections/tumor) were stained. 350–500 EGFP⁺ cells were counted per section. DAPI (blue) staining highlights nuclei. Mean \pm SEM is shown. **(C)** Western blot of P-Stat3-Y705 (P-Stat3) and total Stat3 (Stat3) in mouse neurofibroma (tumor) and wild-type sciatic nerve (WT nerve); blot is representative of neurofibromas (n=5) and wild-type nerves (n=3). **(D)** Representative pictures of immunostaining of P-STAT3(Y705) (left) and β -catenin (right) in human plexiform neurofibroma. In right, black arrow indicates nuclear β -catenin, white arrow indicates cytoplasmic β -catenin, black arrowhead indicates both. **(E)** Distribution of % P-

STAT3 positive neurofibroma cells vs % nuclear β -catenin positive only (blue) or cytoplasmic and/or nuclear β -catenin positive (red) in 30 human plexiform neurofibromas. Spearman correlation coefficient analysis between P-STAT3(Y705) and β -catenin distribution (P-STAT3 vs total beta catenin shown in red, $r=0.7219$, $p<0.0001$; P-STAT3 vs nuclear beta catenin shown in blue, $r=0.6374$, $p=0.0002$, two tailed). (F) Quantification of intensity of P-STAT3(Y705) and β -catenin immune-positive cells in NF1 human plexiform neurofibromas and Spearman correlation coefficient analysis between P-STAT3(Y705) and β -catenin intensity ($r=0.4373$; $p=0.0157$, two-tailed). Bar=10 μ m.

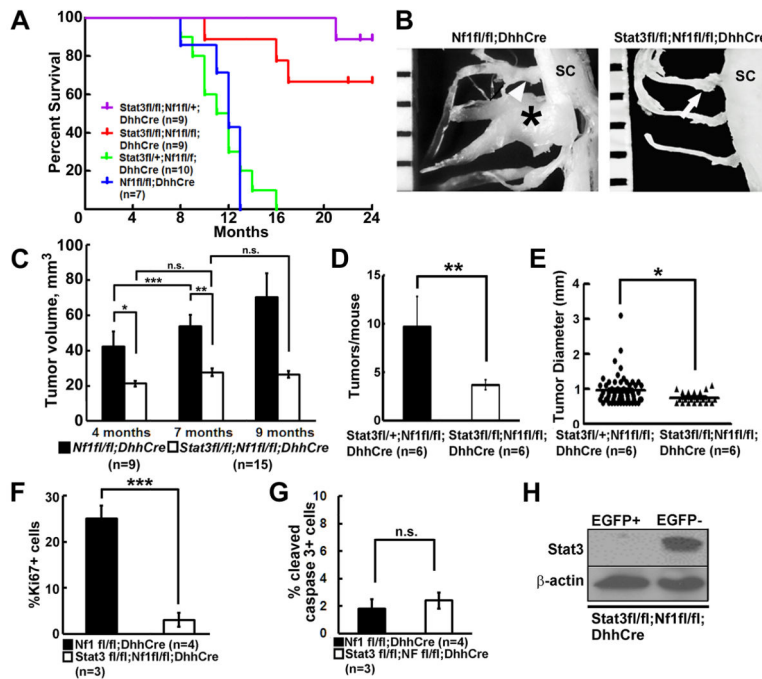


Figure 3. Targeted genetic deletion of Stat3 in SCs and SCPs delays neurofibroma formation in vivo

(A) Kaplan-Meier survival curve. Purple: *Stat3^{fl/fl};Nf1^{fl/+};DhhCre*; Red, *Stat3^{fl/fl};Nf1^{fl/fl};DhhCre*; Blue: *Stat3^{fl/+};Nf1^{fl/fl};DhhCre*. Green *Nf1^{fl/fl};DhhCre*. (B) Representative gross dissections of thoracic paraspinal neurofibromas and nerve roots in 9 month old *Nf1^{fl/fl};DhhCre* (left) and *Stat3^{fl/fl};Nf1^{fl/fl};DhhCre* (right) mice. Ruler shows 1 mm markings. (C) Neurofibroma volumes at 4, 7, and 9 months of age, measured in MRI images. *Nf1^{fl/fl};DhhCre* mice (n=12, black bars) and *Stat3^{fl/fl};Nf1^{fl/fl};DhhCre* mice (n=15, white bars) at 4, 7 and 9 months of age. (D) Average tumor number per mouse at 5 months in the *Stat3^{fl/fl};Nf1^{fl/fl};DhhCre* (white bar, n=6) and littermates *Stat3^{fl/+};Nf1^{fl/fl};DhhCre* mice (black bar, n=6). (E) Tumor diameter in the *Stat3^{fl/fl};Nf1^{fl/fl};DhhCre* (circle, n=6 mice with 57 tumors) and littermates *Stat3^{fl/+};Nf1^{fl/fl};DhhCre* mice (triangle, n=6 mice with 21 tumors). (F) Cell proliferation shown as percent Ki67⁺ cells in *Nf1^{fl/fl};DhhCre* mice (n=4, black bar) and *Stat3^{fl/fl};Nf1^{fl/fl};DhhCre* mice (n=3, white bar). (G) Cell death shown as percent cleaved caspase 3⁺ cells in *Nf1^{fl/fl};DhhCre* mice (n=4, black bar) and *Stat3^{fl/fl};Nf1^{fl/fl};DhhCre* mice (n=3, white bar). (H) Western blot on FACS-sorted EGFP⁺, EGFP⁻ cells dissociated from adult *Stat3^{fl/fl};DhhCre;EGFP^{fl/fl}* mouse sciatic nerves. Statistics: c: Ordinary one way ANOVA, d-g: unpaired student *t* test. *=*p*<0.05, **=*p*<0.01, ***=*p*<0.001, n.s.=not significant.

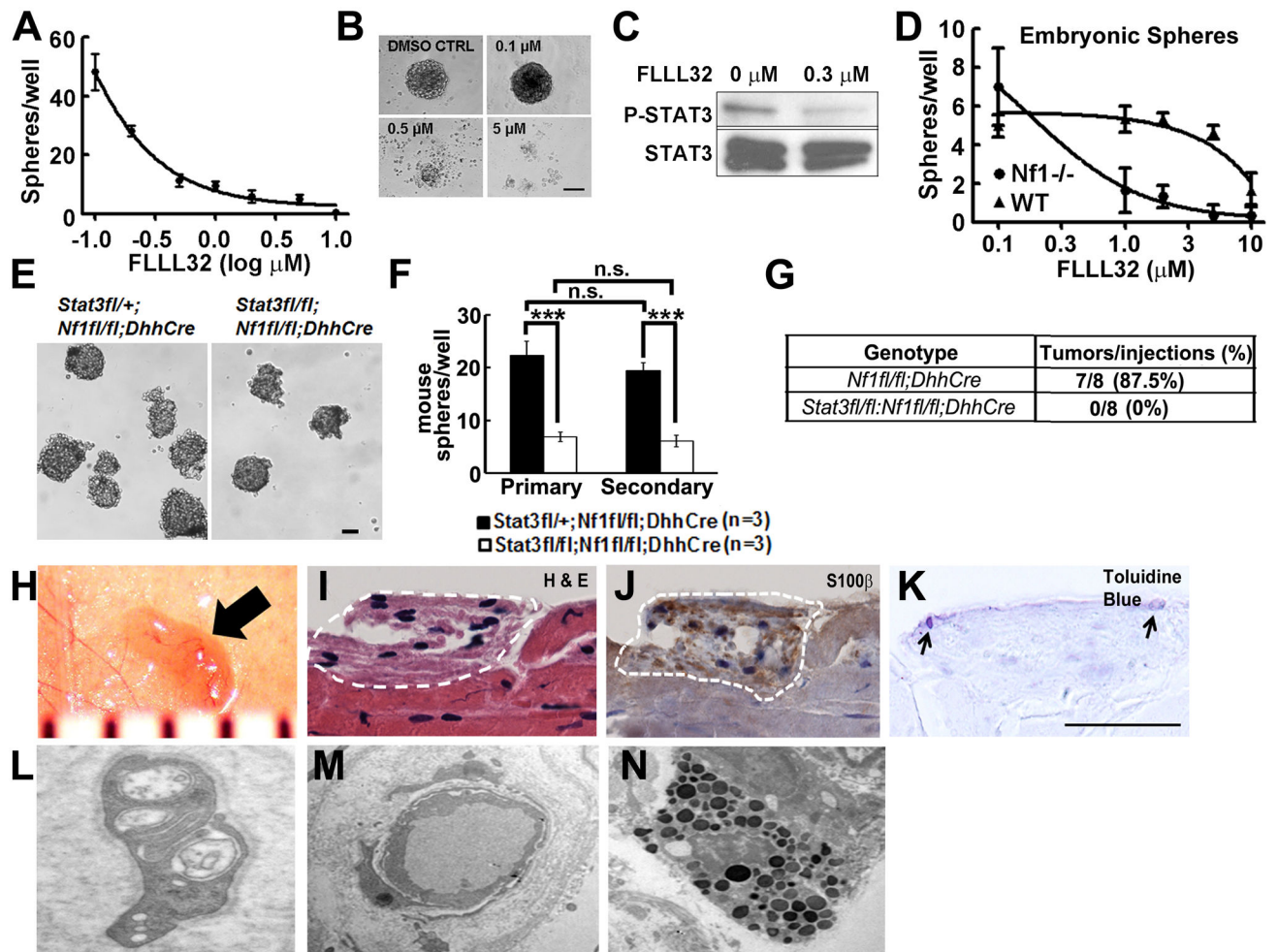


Figure 4. Stat3 contributes to neurofibroma initiation

(A) The JAK2/STAT3 inhibitor FLLL32 inhibits formation of human neurofibroma spheres. DMSO (0) served as control. (B) Phase contrast images of human neurofibroma spheres treated with FLLL32 for 5 days. (C) Western blot of P-STAT3-Y705 and STAT3 in human neurofibroma spheres, +/-0.3 μM FLLL32. (D) Low doses of FLLL32 inhibit formation of mouse E12.5 *Nf1*^{-/-} spheres; effects on E12.5 wild-type spheres are observed only at higher concentrations. (E) Phase contrast images of primary neurofibroma/DRG spheres from *Stat3*^{fl/+}; *Nf1*^{fl/fl}; *DhhCre* mice (left; control) and *Stat3*^{fl/fl}; *Nf1*^{fl/fl}; *DhhCre* mice (right). (F) Primary and secondary neurofibroma/DRG sphere number is reduced in the absence of Stat3 (n=3/group). (G) Neurofibroma-like lesions form after subcutaneous injection of *Nf1*^{fl/fl}; *DhhCre* neurofibroma sphere cells but not in *Stat3*^{fl/fl}; *Nf1*^{fl/fl}; *DhhCre* mouse derived neurofibroma sphere cells. (H) Gross photograph of a lesion (black arrow) under reflected skin in a mouse injected with *Nf1*^{fl/fl}; *DhhCre* neurofibroma sphere cells. Ruler shows 1 mm markings. (I) H & E stained section of F; lesion is indicated by white dotted line. (J) Immunohistochemistry showing S100β⁺ cells (brown) in tumor. Blue is hematoxylin counterstain. (K) Toluidine blue staining showing mast cells (black arrow). On EM, lesions contain SCs, identified by continuous basal lamina and wrapping of small axons (L), blood

vessels (**M**) and mast cells (**N**). Bar=50 μ m B and E, others bar=20 μ m. Statistics: Ordinary one way ANOVA.

Author Manuscript

Author Manuscript

Author Manuscript

Author Manuscript

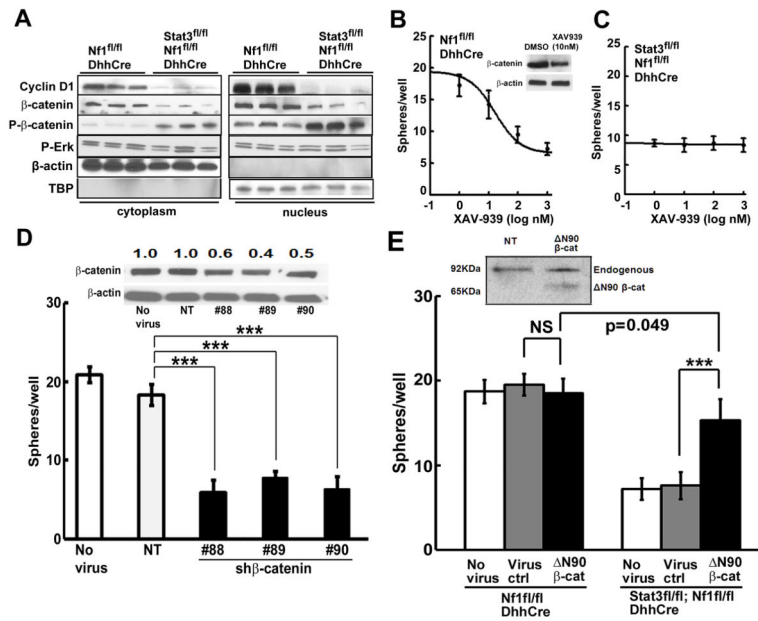


Figure 5. β-catenin signaling is a critical indicator of Stat3 in neurofibroma

(A) Western blots of nuclear and cytoplasmic proteins from *Stat3^{fl/fl};Nf1^{fl/fl};DhhCre* or *Nf1^{fl/fl};DhhCre* mouse neurofibromas/DRGs with indicated antibodies. (B) β-catenin tankyrase inhibitor XAV-939 inhibits formation of *Nf1^{fl/fl};DhhCre* mouse neurofibroma spheres. DMSO (0) was control. Insert: 10nM XAV-939 inhibited β-catenin expression by 3 days. (C) Low dose XAV-939 has no effect on the formation of *Stat3^{fl/fl};Nf1^{fl/fl};DhhCre* mouse neurofibroma spheres. (D) Three shβ-catenin shRNAs (#88, #89, and #90) each decrease mouse neurofibroma sphere formation, versus non-target lentivirus YFP (NT) or no virus controls. Insert shows Western blot confirming shβ-catenin-mediated knock down of total β-catenin. Anti-β-actin is loading control. Numbers show the ratio of β-catenin to β-actin loading control, then to no virus expression level. (E) Overexpression of β-catenin deltaN90 (N90) in *Stat3^{fl/fl};Nf1^{fl/fl};DhhCre* mouse neurofibroma/DRG spheres increased sphere numbers (black) versus virus (grey, p<0.001) or no virus controls (white, p<0.001). Overexpression of N90 β-cat in *Nf1^{fl/fl};DhhCre* mouse neurofibroma/DRG spheres did not significantly increase sphere numbers (black) versus virus (grey, p=0.15) or no virus (white, p=0.43). Insert: Western blot detects endogenous 92KDa β-catenin and ~60KDa of overexpression of mutated N90 β-cat in *Stat3^{fl/fl};Nf1^{fl/fl};DhhCre* mouse neurofibroma spheres. Statistics: Ordinary one way ANOVA. Three independent experiments were performed in B, C and E.

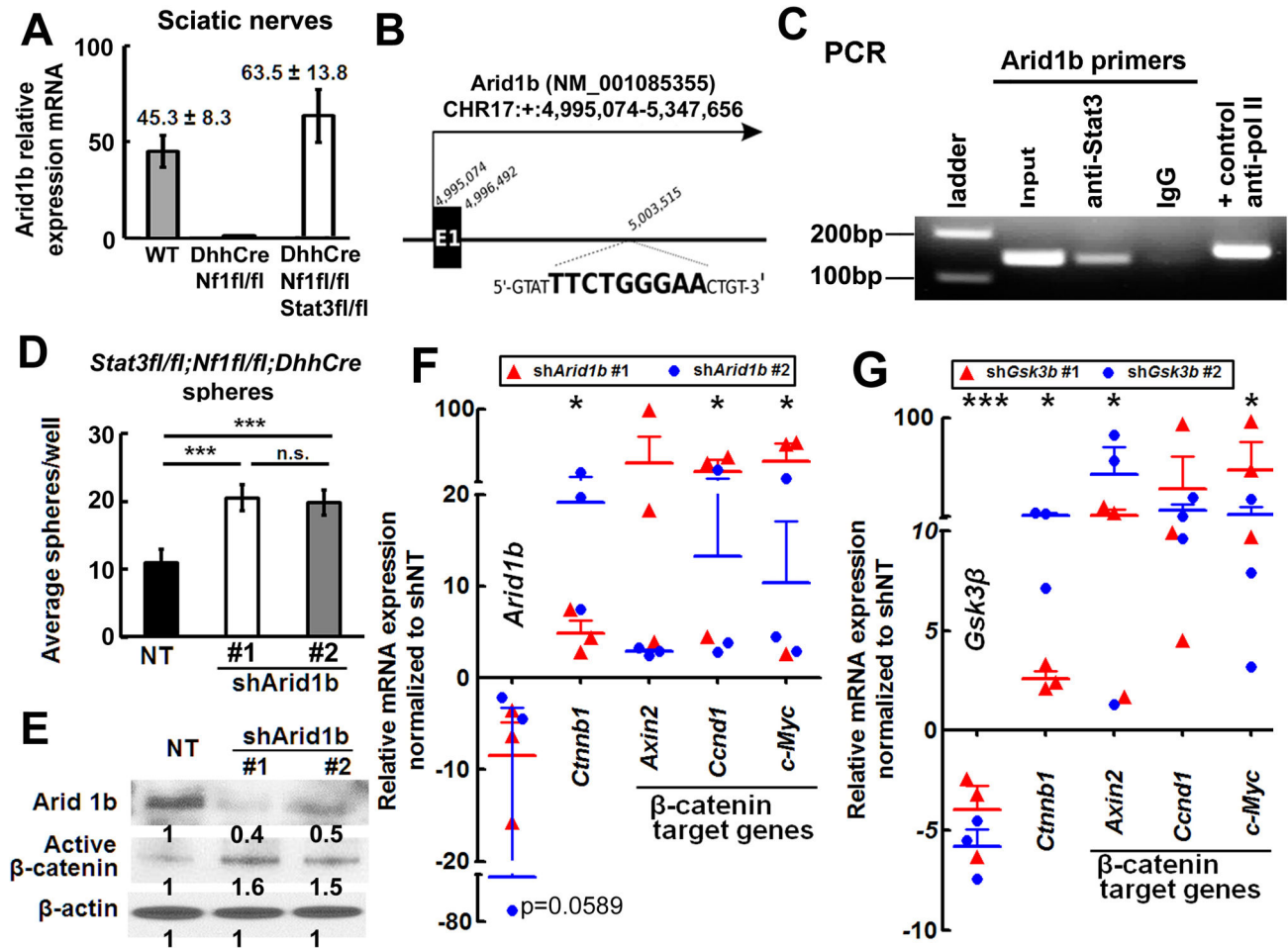


Figure 6. Stat3 transcriptionally represses Arid1b expression, activating β-catenin
 (A) qRT-PCR shows high *Arid1b* mRNA in *Stat3^{fl/fl};Nf1^{fl/fl};DhhCre* mouse sciatic nerve (white, n=6) versus WT (n=6) and *Nf1^{fl/fl};DhhCre* nerve (n=6). (B) Schematic, exon 1 mouse *Arid1b* gene. A putative Stat3 binding motif is between Exon 1 and Exon 2; the binding motif sequence is shown in bold. (C) Stat3 on the *Arid1b* promoter. PCR amplified a 139-bp *Arid1b* DNA fragment after ChIP with anti-Stat3. IgG was negative control. (D) Two *Arid1b* shRNAs increase numbers of *Stat3^{fl/fl};Nf1^{fl/fl};DhhCre* mouse neurofibroma spheres. (E) Western blot shows knockdown of Arid1b and increased β-catenin in *Stat3^{fl/fl};Nf1^{fl/fl};DhhCre* mouse neurofibroma spheres 4 days after sh*Arid1b* infection in two different shRNA clones. (F–G) β-catenin target gene expression increases after sh*Arid1b* (F) or sh*Gsk3β* (G) infection of *Stat3^{fl/fl};Nf1^{fl/fl};DhhCre* neurofibroma spheres. Mean ± SEM is shown for 3 independent experiments and 2 clones of shRNA in D, F and G. A representative experiment (of 3) is shown in C. Statistics: Ordinary one way ANOVA.

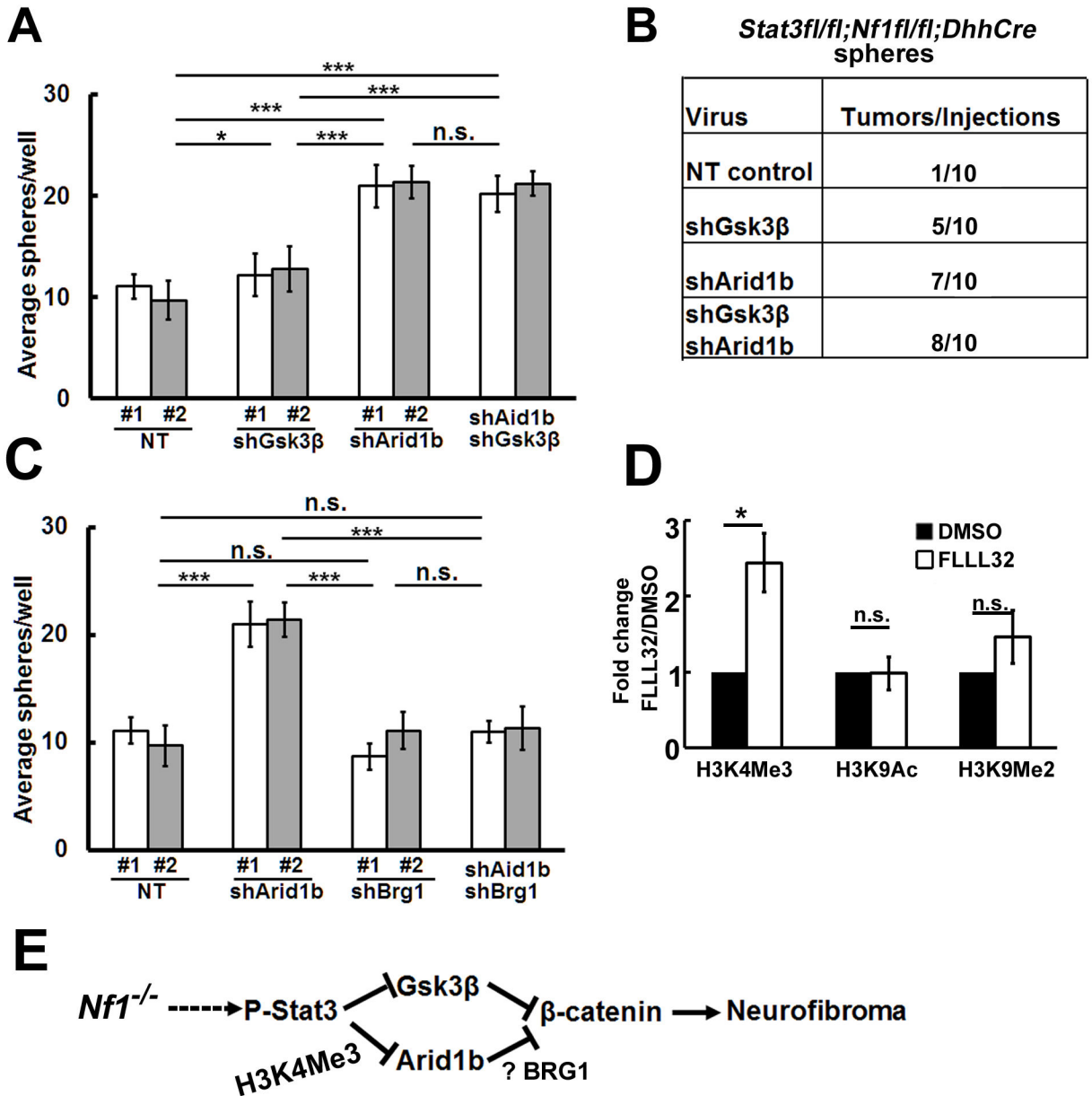


Figure 7. *Arid1b* and *Gsk3β* contribute to *Stat3* mediated neurofibromagenesis

(A) *In vitro*, *shGsk3β* does not fully rescue *Stat3^{fl/fl};Nf1^{fl/fl};DhhCre* sphere numbers. Simultaneous knockdown of *Gsk3β* and *Arid1b* shows similar effects to *shArid1b* alone. (B) Neurofibroma-like tumors form in *Stat3^{fl/fl};Nf1^{fl/fl};DhhCre* sphere cells infected with *shArid1b*, *shGsk3β*, or both and transplanted into *nu/nu* mice. (C) *Brg1* is necessary for *Stat3^{fl/fl};Nf1^{fl/fl};DhhCre* sphere formation in cells treated with *shArid1b*. (D) CHIP shows enhancement of the H3K4Me3 mark at the *Arid1b* promoter. (E) Schematic shows a model of neurofibroma initiation: Loss of *Nf1* in SCP causes activation of P-Stat3. P-Stat3 transcriptionally represses *Arid1b* and *Gsk3β*, increasing β-catenin activity. Mean ± SEM is shown for 3 independent experiments in Panels A, C, and D. Two different shRNA clones (#1 and #2) were used in A and C, For combination, we used *shArid1b* #1+*shGsk3β* #1

(white bar) or shArid1b #2+shGsk3 β #2 (grey bar) in A. We used shArid1b #1+shBrg1 #1 (white bar) shArid1b #2+shBrg1 #2 (grey bar) on C. Statistics: Ordinary one way ANOVA.

Author Manuscript

Author Manuscript

Author Manuscript

Author Manuscript